ADVANCED FUNCTIONAL MATERIALS
www.afm-journal.de

A Structural Gel Composite Enabled Robust Underwater Mechanosensing Strategy with High Sensitivity

Zibi Wang, Honghao Zhou, Dong Liu, Xue Chen, Ding Wang, Sheng Dai, Fei Chen, and Ben Bin Xu**

One of the key challenges in developing gel-based electronics is to achieve a robust sensing performance, by overcoming the intrinsic weaknesses such as unwanted swelling induced deformation, signal distortion caused by dehydration, and large hysteresis in sensing signal. In this work, a structural gel composite (SGC) approach is presented by encapsulating the conductive hydrogel/MXene with a lipid gel (Lipogel) layer through an in situ polymerization. The hydrophobic Lipogel coating fulfills the SGC with a unique anti-swelling property at an aqueous environment and excellent dehydration feature at an open-air, thus leading to long-term ultra-stability (over 90 days) and durability (over 2000 testing cycles) for underwater mechanosensing applications. As a result, the SGC based mechanoreceptor demonstrates high and stable sensitivity (GF of 14.5). Moreover, several SGC based conceptual sensors with high sensitivity are developed to unveil their profound potential in underwater monitoring of human motions, waterproof anti-counterfeiting application, and tactile trajectory tracking.

1. Introduction

Responsive hydrogel based smart technology recently emerges with huge promises in future engineering applications as mechanosensation,[1–3] soft robots[4–7] and energy storage,[8–10] owing to their distinctive solid-like mechanical elasticity and liquid-like transporting behavior.[11] In particular, the hydrogel-based wearable device can facilitate unique skin-like mechanical properties mediated by the conformal interaction and high sensitivity.[12,13] One of the merits for wearable mechanosensor is whether it can maintain robust sensing performance at aquatic conditions (i.e., sweating, raining, swimming and sub-sea conditions).[14,15] As well known, the hydrogel can easily undergo swelling at hydrated environment, thus lead to the unwanted deformation, distortion/disruption in output signal and irreversible degradation/damage on overall properties.[16,17] The hydrogel-based electronics that can work robustly in the hydrated environment is highly desired and remains yet to achieve.

Persistent efforts have been devoted to deliver anti-swelling capability for hydrogel by introducing hydrophobic segments,[18–20] elaborating high crosslinking density,[21,22] and/or constructing fully hydrophobic environment.[23–25] Gao and co-workers[20] constructed a hydrogel-based wearable sensor via the copolymerization of hydrophilic and hydrophobic monomers in a mixed solvent consisting of water and dimethyl sulfoxide (DMSO), which demonstrates outstanding anti-swelling and sensing features. Unfortunately, the miscibility between DMSO and water initialized the uncontrollable immigration of molecules to deteriorate the carrier transport path, therefore lead to the loss of sensitivity. Wu et al.[25] developed an ionogel sensor with an excellent anti-swelling capability and no explicit molecule exchanges between gel and external environment. However, low conductivity and inconsistent sensitivity appeared as the nonaqueous medium and strong molecular interactions severely restrain the immigration of ions. The way to forge anti-swelling feature with high sensitivity for hydrogel-based sensor awaits to be explored.

Inspired by the mammalian skin constituted by the hydrophilic dermis and hydrophobic epidermis,[26,27] researcher generated the concept to generate a hydrophobic isolation layer on the hydrogel to achieve anti-dehydration and anti-swelling capabilities, by blocking the mass transfer pathway between the hydrogel and surrounding.[28–30] Nevertheless, considerable technical gaps need to be bridged to construct the hydrophobic layer on the surface without altering the bulk hydrogel structure.[31] Due to the incompatible mechanical properties and weak bond on the hydrophobic coating/hydrogel

Z. Wang, D. Liu, F. Chen
School of Chemical Engineering and Technology
Xi'an Jiaotong University
No. 28, Xianning West Road, Xi'an, Shaanxi 710049, P. R. China
E-mail: feichen@xjtu.edu.cn
H. Zhou, X. Chen, B. B. Xu
Mechanical and Construction Engineering
Faculty of Engineering and Environment
Northumbria University
Newcastle upon Tyne NE1 8ST, UK
E-mail: ben.xu@northumbria.ac.uk
D. Wang
Faculty of Engineering and Physical Sciences
University of Southampton
University Road, Southampton SO17 1BJ, UK
S. Dai
School of Chemical and Process Engineering
University of Leeds
Leeds LS2 9JT, UK

The ORCID identification number(s) for the author(s) of this article can be found under https://doi.org/10.1002/adfm.202201396.

DOI: 10.1002/adfm.202201396

interface,[28] the obtained gel composite usually presents limited stretchability and low mechanical strength, as well as other drawbacks such as low/unstable conductivity and insufficient adhesion at underwater condition.[32,33]

Herein, we describe a structural gel composite (SGC) strategy by creating a hydrophobic lipid gel (Lipogel) layer in situ on the hydrogel/MXene core. The obtained SGC contains a robust Lipogel/hydrogel interface to realize the stable mechanical performance and the integral hydrogel/MXene structure, where the Lipogel layer is anchored on the hydrogel surface with an adjustable thickness (up to 200 µm). The SGC presents ultra-stability for mechanical property both in the open air and underwater, reliable underwater sensing capability with high accuracy and faster responsiveness. A flexible SGC based mechanoreceptor is achieved with a high sensitivity (GF of 14.5). We also demonstrate a series of SGC based sensors to perform instantaneously and logical tactile sensing at underwater environment.

2. Results and Discussion

The SGC by wrapping the conductive hydrogel/MXene with a hydrophobic lipid gel (Lipogel) layer, was synthesized through the in situ polymerization (**Figure 1**). The conductive hydrogel/MXene is prepared (Figure 1a,b and Figure S1, Supporting Information) through the copolymerization of acrylic acid (AA), 2-hydroxyethyl acrylate (HEA), and MXene nanosheets (Figure S2, Supporting Information) in the aqueous solution at room temperature (Figure S3, Supporting Information).[34] Compared with PAA hydrogel, the poly (AA-*co*-HEA)-MXene hydrogel hybrid (PAHM) show intensive micropores (Figure S4, Supporting Information), suggesting a high cross-linking interactions between polymer chains and MXene nanosheets. After treatment, unsaturated double bonds are introduced on the surface of PAHM (Figure 1c) through the reaction between the surface hydroxyl groups and the acryloyl chloride (Figure S5, Supporting Information).[35]

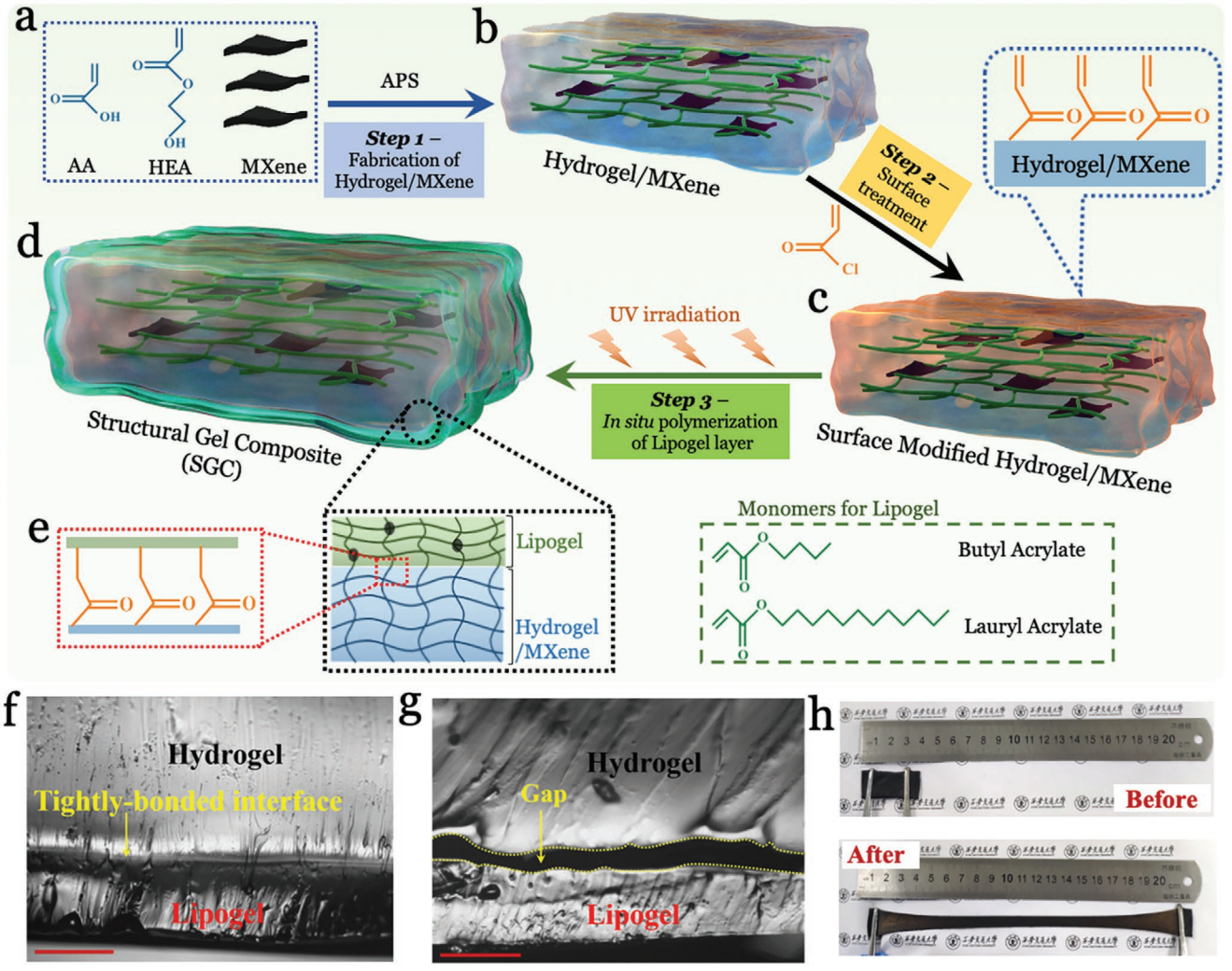

Figure 1. The fabrication of structural gel composite (SGC) with robust interface. a) Monomers for synthesizing Hydrogel/MXene hybrids (PAHM). b) Illustration of PAHM. c) Illustration of surface modification of PAHM. Illustrations of d) SGC and e) the interface between Lipogel (with monomers for synthesizing Lipogel) and PAHM. Optical microscopic images on the cross-section of SGC f) with and g) without modification. Scale bar: 100 µm. h) Demonstration of the stretchability for PAHM-8%.

The ethyl acetate is utilized as the solvent to ensure the reaction only occurs on the surface of hydrogel/MXene, due to its poor miscibility with water. The FTIR results in Figure S6 (Supporting Information), confirm the completion of surface treatment with the existences of double bonds, with the characteristic peaks appearing at 3007, 1403, and 981 cm^{-1} in SM-PAHM hydrogel and the shift of −OH peaks from 3343 to 3392 cm^{-1}.

The hydrophobic Lipogel layer was synthesized by in situ copolymerizing the hydrophobic acrylate monomers with vinyl groups (Figure 1d and Figure S7, Supporting Information) in a hydrophobic medium—paraffin oil, which is immiscible with water, to support the formation of Lipogel layer on the hydrogel surface. Compared with the FTIR spectra of SM-PAHM hydrogel (Figure S6, Supporting Information), the disappearance of double bond peaks in SGC and new $-CH_3$ and $-CH_2$ peaks at 2925 and 2855 cm^{-1} verify the covalent linkage on the Lipogel/hydrogel interface (Figure 1e). In Figure 1f, we find that the hydrophobic Lipogel is tightly anchored on the hydrogel surface without any delamination. Meanwhile, the observation for PAHM/Lipogel composite without surface modification by acryloyl chloride, reveals distinct gap on the interface due to the incompatibility between Lipogel and hydrogel (Figure 1g), which causes the slippery fracture of materials in the later stress–strain test (Figure S8, Supporting Information). By characterizing the interfacial strength between Lipogel and hydrogel/MXene (Figure S9 and Movie S1, Supporting Information), an excellent interfacial strength of ≈395 J m^{-2} is found for SGC, which is 415 folds of the interfacial strength value (≈0.95 J m^{-2}) for the Lipogel and hydrogel/MXene interface without treatment. Further observation indicates that the Lipogel layer can uniformly encapsulate the hydrogel/MXene from all directions (Figure S10, Supporting Information). Whereas the thickness of Lipogel layer can be adjusted from 20 to 200 μm, the thickness was set as 100 μm for the following studies, after considering the overall mechanical property (Figure S11, Supporting Information). After practicing a brief assessment of stretchability on SGC (Figure 1h), an excellent elongation (1000% stretching strain) is discovered.

The mechanical properties of SGC are subsequently studied as a function of the concentration of MXene. The tensile strength increases with the addition of MXene and the optimal toughness with excellent stretchability is obtained at 8 wt% MXene (Figure S12, Supporting Information). This enhancement is contributed by the effective energy dissipation induced by the dynamic noncovalent interactions between MXene and polymer networks (Figure S13, Supporting Information).[34] The impact on mechanical property of SGC from the Lipogel layer is examined with different lauryl acrylate (L)/butyl acrylate (B) monomers ratio. In **Figure 2**a and Figure S14 (Supporting Information), both the fracture strain and toughness of SGC increase when L/B increases. The SGC with a L/B of 90% presents a high elongation of 1380%, because the short alkane side chains (4 C) in B brings rigidity and strength and the long alkane side chains (12 C) in L fulfill the flexibility to Lipogel.[36] The Lipogel with an L/B of 90% is selected for the following studies. Due to the low mechanical strength (Figure S15, Supporting Information), the introduction of Lipogel brings the peak stress down by 10% for SGC (Figure 2b), but the elongation has been well maintained (less than 3% reduction). The SGC presents a rapid recovery of 95% of its toughness within 20 min after applying 300% tensile strain (Figure 2c), an outstanding reproducibility during the cyclic tests (Figure S16a, Supporting Information) and a good antifatigue property based on the loading-unloading curves in Figure S16b (Supporting Information).

In Figure 2d, the SGC exhibits a brilliant anti-swelling feature with negligible swelling ratio (≈3%) after 200 h, due to the protection of Lipogel layer. In contrast, the swelling ratio of hydrogel/MXene rapidly increases to 540% (50 h), then the sample collapses (Figure S17, Supporting Information). The microscopic observation for SGC after 200 h of immersion (Figure S18a, Supporting Information) reveals a homogeneous morphology, same as the original structure (Figure S4b, Supporting Information). However, the pores are deformed significantly in the hydrogel/MXene due to the swelling (Figure S18b, Supporting Information). The tensile testing results uncovers a long-term underwater mechanical stability for SGC by retaining over 80% of original elastic modulus, fracture strain, tensile strength and toughness after immersing in water for 200 h (Figure 2e). The SGC presents an extraordinary resilience after 300 underwater tensile cycles, as no deterioration/change is detected on the interface between Lipogel and hydrogel/MXene (Figure S19, Supporting Information), on the outer surface of SGC (Figure S20a,b, Supporting Information) and even the swelling behavior (Figure S20c, Supporting Information).

To quantify this effective water resistance from Lipogel layer, we perform the surface contact angle analysis. The hydrogel/MXene surface shows a typical hydrophilic status with a water contact angle (WCA) of 23.6° ± 1.2° (Figure S21, Supporting Information), the SGC surface presents a WCA of 115.4° ± 3.8° due to the hydrophobic nature of Lipogel layer. Our hypothesis is that the long alkyl chains of L would preferentially accumulate on the Lipogel surface[37] when the SGC is soaked in water, due to the incompatibility between water and hydrophobic alkyl chains,[23] then the long alkyl chains coil to form a dense hydrophobic network with lower surface free energy, thus realizing the long-term stability of SGC (Figure 2f). To verify above hypothesis, we compare the WCA for SGC with different L/B ratio. The WCA of SGC explicitly increases with the increment of L monomer, and reaches 129.2° ± 3.9° for the WCA of Lipogel coating made by L only (Figure 2g), indicating that the surface with long alkyl chains is more hydrophobic as a result of longer alkyl chains.[38] Interestingly, the SGC becomes more hydrophobic with showing a WCA of 137.4° ± 4.9° after soaking in water for 24 h (Figure 2h), which indicates that the hydraulic coiling of alkyl chains happens and increases the capability to resist water molecules to diffuse into the hydrogel/MXene area, to facilitate long-term underwater stability. This hydraulic coiling of alkyl chains occurs both on the Lipogel/water and Lipogel/hydrogel MXene interface (Figure S22, Supporting Information), the enhancement in hydrophobicity (118.9° ± 5.8°) at Lipogel/hydrogel MXene interface after immersing for 24 h seems incremental due to the limited water interaction, where most water molecules are locked by the hydrogel

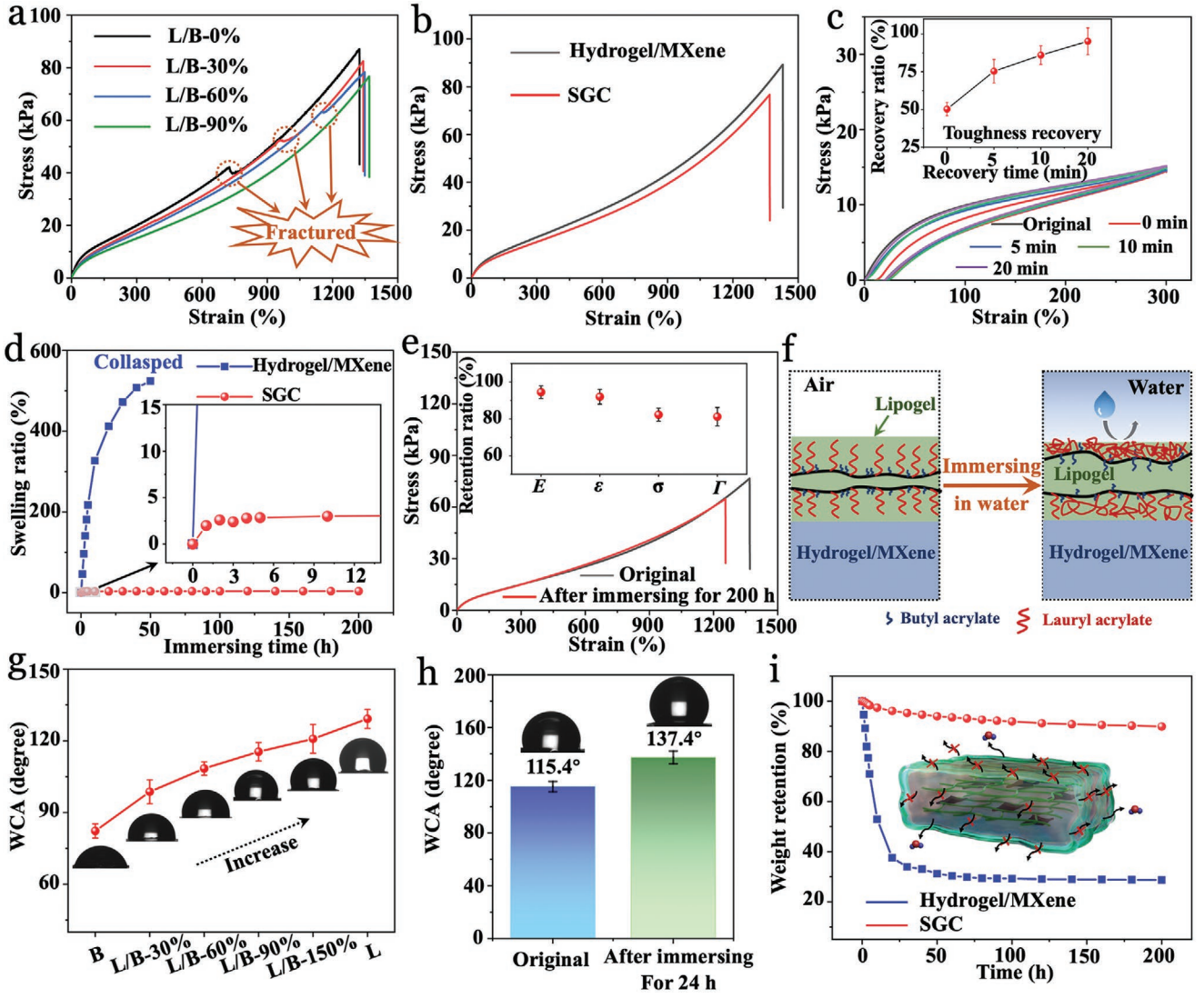

Figure 2. Characterization of mechanical and surface properties. a) Stress–strain curves of SGC with various L/B. b) Stress–strain curves of hydrogel/MXene and SGC. c) Self-recovery behavior of SGC. d) Swelling behavior of hydrogel/MXene and SGC. e) Stress–strain curves comparison of SGC after immersion of 200 h, and the corresponding retention ratio of elastic modulus (E), fracture strain (ε), tensile strength (σ), and toughness (Γ). f) Schematic illustration of hydrophobic chains accumulation of SGC after immersing in water. g) WCA of SGC with different L/B. h) WCA of original Lipogel surface and the surface after immersion of 24 h. i) Water retentions of hydrogel/MXene and SGC at open air.

polymer network. Interestingly, this incremental enhancement in hydrophobicity can effectively preserve the SGC in the open air from dehydration (Figure 2i), as the SGC can sustain over 90% of its original weight after 200 h when the hydrogel/MXene present about 70% weight loss within 50 h.

While a variety of strategies have been proposed to enhance the adhesion of gel,[39] limited attentions have been paid to the long-term underwater adhesion.[32] By exercising on the substrates include glass, copper, rubber, tinplate, carnelian, wood, polyethene (PE) and polytetrafluoroethylene (PTFE), it is interesting to find that the SGC can adhere to all substrates both in the open air and underwater (**Figure 3**a,b). The adhesion strength test (Figure 3c), shows a robust adhesion performance (Figure 3d, Figure S23a,b, Supporting Information). The SGC even possesses stronger underwater adhesion on the hydrophobic substrates (PTFE, PE) than the hydrophilic ones (glass, copper, pigskin and rubber). The reason probably is that the functional groups on the surface of hydrophilic substrates are likely to be defuncted in water. Our SGC can retain stable adhesion strength even after 8 repeatedly pasting-peeling cycles both in the open air and underwater (Figure 3e). Moreover, the SGC presents no noticeable decline in adhesion when stored for 5 h (Figure 3f) both in the open air and underwater. By studying the adhesion strength of SGC as function of varied L/B (Figure 3g), we find that the adhesion increases substantially when increasing the concentration of L, which agrees well with the previous report.[40] When adhering to substrates underwater, the long alkyl chains of L units (Figure S24, Supporting Information) accumulate to expel the hydrated overlayer on the surface, and adhere to substrates via hydrophobic interactions,

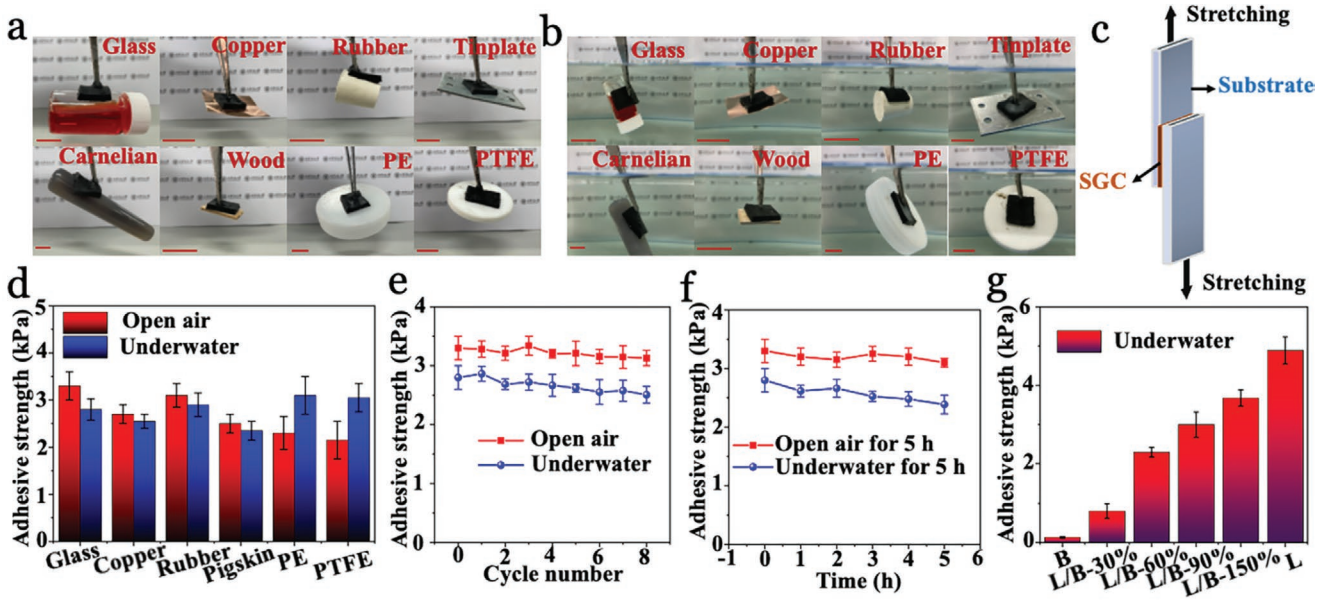

Figure 3. Characterization of adhesion. Adhesion demonstration of SGC on various substrates: a) in the open air after 5 h and b) underwater after 200 h, scale bar: 1 cm. c) The sketch for adhesion testing set-up. d) Adhesive strength for various substrates. e) Adhesion strength for glass for 8 cycles. f) Adhesion strength for glass after storing in air and underwater for 5 h. g) Adhesion strength for SGC on glass with various L/B.

dipole-dipole interactions and hydrogen bonds.[25] By comparing with the published works (Table S1, Supporting Information), there are substantial room to improve the underwater adhesion for our SGC, therefore, we will aim to focus this part of research in the future work.

We next evaluate the underwater mechanosensing behavior for SGC (**Figure 4**a). The SGC presents a high sensing sensitivity at a broad strain range (0–1000%), where the gauge factor (GF) is defined as GF $= (\Delta R/R_0)/\varepsilon$.[41] A nonlinear segmental trend for $\Delta R/R_0$ is summarized with three linear sections ($R^2 \geq 0.99$) per strain range: a GF of 4.135 for 0–200% strain, a GF of 8.015 for 200–500% strain and a GF of 14.507 for the strain range of 500–1000%. The sensitivity of our SGC is significantly higher than the other reported hydrogel-based sensors (Table S2, Supporting Information), owning to the effective interconnection points between MXene nanosheets (Figure S25a, Supporting Information) to provide optimized electron transmission paths (Figure 4b, Figure S26, Supporting Information). Under stretching, the distance between MXene nanosheets in SGC increases and the corresponding contact areas decrease, resulting into the disruption of electron transmission paths and remarkable reduction in resistance (Figure 4b and Figure S25b, Supporting Information), which endows the high sensitivity for SGC. The strain-responsiveness results of SGC (Figure 4c), indicate that the electrical sensing outputs can be precisely perceived at either a low strain (0.2–2%) or a high deformation (50–500%). The SGC can accurately monitor and distinguish various frequency from 0.04 to 0.32 Hz (Figure S27a, Supporting Information), and also presents prominent reversibility and good recovery during the stretching-holding process (Figure S27b, Supporting Information). In addition, our SGC demonstrates a responsive time of 163.1 ms and a recovery time of 178.8 ms (Figure 4d and Figure S28a, Supporting Information), which are 32.2% and 27.4% lower than the uncoated hydrogel/MXene, respectively. The further testing results (Figure S28b, Supporting Information) suggest that our SGC has achieved an increment of 28.6% in sensitivity compared to the uncoated hydrogel/MXene. The above enhancements in accuracy and responsiveness are attributed to the Lipogel layer enabled conformal attachment to skin, which allows the hydrogel/MXene core to detect the localized deformation timingly.[42]

The SGC also demonstrates a reliable sensing performance with stable electrical outputs. The results of relative resistance at 10% strain for SGC in Figure 4e, indicate no apparent change in sensing outputs after immersing in water for 50 h (≈5% loss). On the contrary, a significant decrease of electrical signal (over 70% after an immersion time of 50 h) with severe distortion is detected for the hydrogel/MXene. The cyclic mechanosensing test at a strain of 100% over 300 times in open air, reveals a reproducible and robust strain-dependent $\Delta R/R_0$ changes (Figure 4f) for SGC. At a lower strain of 5% (Figure S29a, Supporting Information), the $\Delta R/R_0$ appears with a reproducible pattern for 300 cycles. However, the cyclic sensing signals for hydrogel/MXene without the Lipogel layer are significantly offset for both strains of 5% and 100% (Fig 4g and Figure S29b, Supporting Information) at the open air, due to the dehydration. After being stored for 3 months in the open air, SGC still performs robust strain-dependent $\Delta R/R_0$ at 5% and 100% strains (Figure S29c,d, Supporting Information), as the hydrogel/MXene core has been well preserved by the Lipogel layer. The SGC even achieve constant and reproducible $\Delta R/R_0$ output signals after 2000 underwater tensile cycles without decay at 5% strain (Figure 4h) and 100% strain (Figure S29e, Supporting Information), with no structural damage observed for the sample after underwater cyclic test (Figure S30, Supporting Information). For the hydrogel/MXene, irregular and inconsistent output signals appear during the underwater

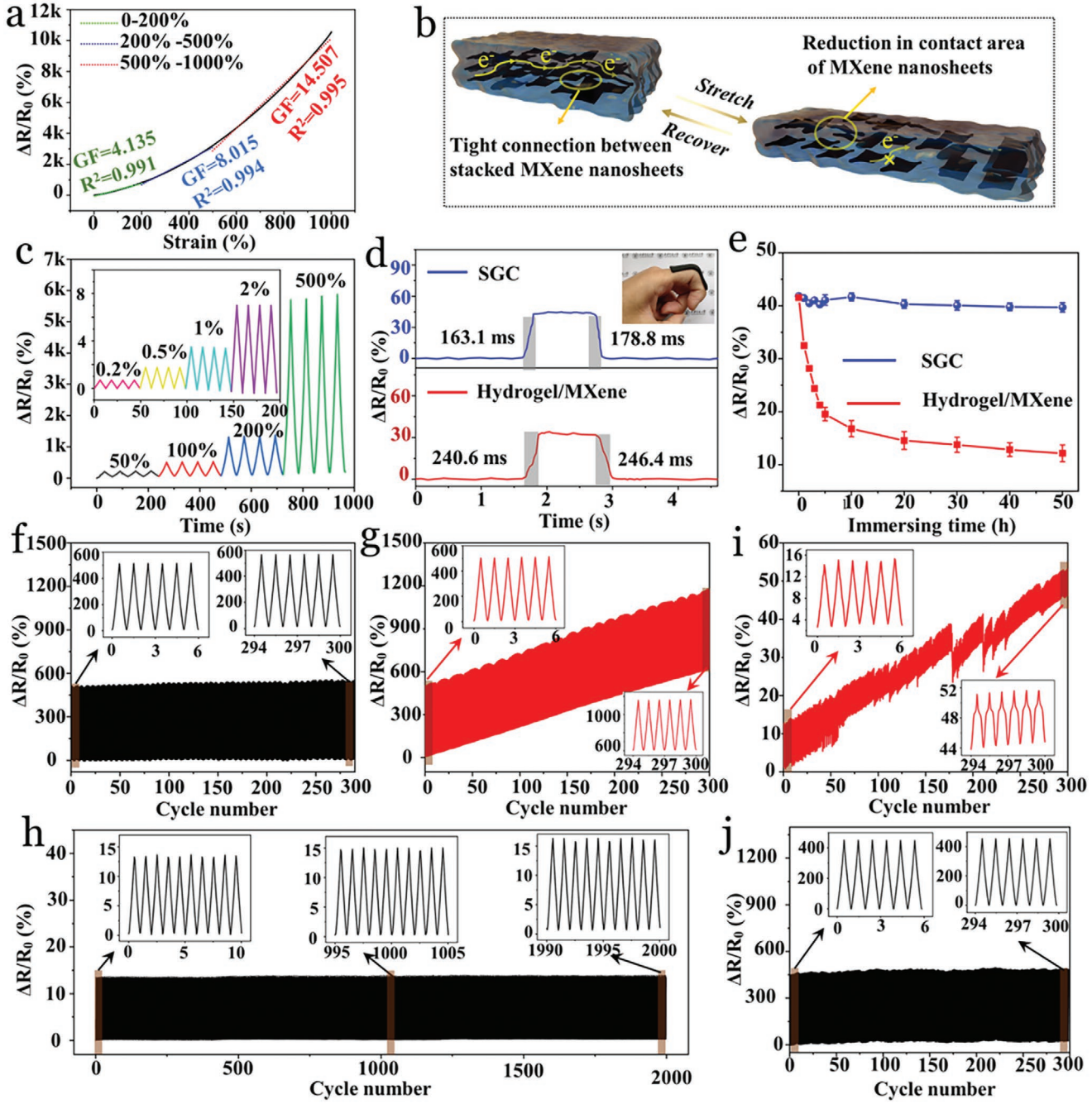

Figure 4. The realization of mechanosensation. a) Gauge factor of SGC based sensor. b) Schematic illustration of the change of MXene nanosheets upon stretching. c) $\Delta R/R_0$ of SGC based sensor under different strains. d) Response and recovery time of SGC and hydrogel/MXene sensors. e) The $\Delta R/R_0$ of hydrogel/MXene and SGC after being immersed in water for certain time period. Cyclic sensing measurements of f) SGC and g) hydrogel/MXene at 100% strain for 300 cycles in open air. Cyclic sensing measurement of h) SGC for 2000 underwater tensile cycles at 5% strain and i) hydrogel/MXene for 300 underwater tensile cycles. j) Cyclic sensing measurement of SGC (stored underwater for 3 months) under 100% strain for 300 cycles.

cyclic testing at 5% strain (Figure 4i), due to the swelling. The hydrogel/MXene sample breaks after 200 cycles at a strain of 100% (Figure S29f, Supporting Information). After being stored in water for 3 months, the SGC maintain stable and robust $\Delta R/R_0$ outputs with negligible degradation (Figure S29g, Supporting Information and Figure 4j).

We next develop a few conceptual devices for underwater mechanosensing. A SGC-based wearable strain sensor is first designed to detect joint/finger movements at underwater environment, such as the bend of finger to 90° (**Figure 5**a and Movie S2, Supporting Information). This wearable sensor can create logic signals in response to various bending degrees

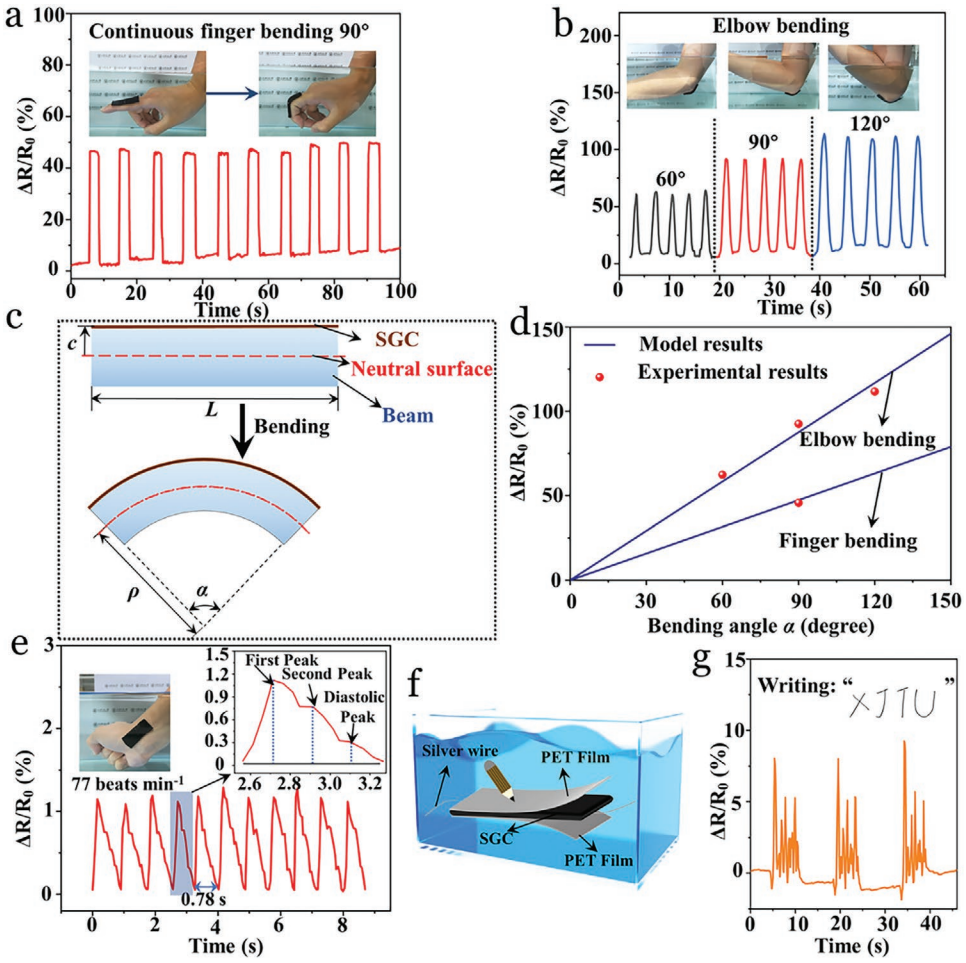

Figure 5. The SGC based underwater sensors. Strain sensor to detect a) finger bending and b) elbow bending with various degrees. c) Numerical modeling of SGC based strain sensor under bending: a beam model with a layer of SGC adhered to the surface (top); beam bending (bottom). d) Bending angle–resistance response. e) A pulse detector. f) Schematic illustration of handwriting system. g) $\Delta R/R_0$ for the letter of "XJTU."

(60°/90°/120°, Figure 5b) when applied on the elbow. The underlying mechanics can be interpreted based on a beam model with a SGC layer adhering on the surface (Figure 5c). Upon bending, the top surface of beam elongates and the resulted strain ε of the SGC can be estimated as $\varepsilon = \frac{c}{\rho}$, with c being the distance between the top beam surface and its neutral surface, and ρ being the radius of deformed beam. The bending angle α (in radian) can be calculated as $\alpha = \frac{L}{\rho}$, where L is the beam length. Thus, we can derive $\varepsilon = \frac{c}{L}\alpha$. The strain ε results in an increase in the resistance of SGC due to the increased distance between MXene nanosheets and the reduced contact area of these sheets. Under a small strain (<200%), we have already obtained a linear relationship (Figure 4a) between $\Delta R/R_0$ and ε as $\Delta R/R_0 = GF \times \varepsilon$, at a GF of 4.135. Therefore, the bending angle–resistance relationship can be expressed as $\Delta R/R_0 = GF\frac{c}{L}\times\alpha$. Given $\frac{c}{L} \approx 0.073$ for finger and $\frac{c}{L} \approx 0.135$ for elbow, the numerical modeling for mechanosensing at bending condition can be obtained in Figure 5d (radian is converted to degree), where a good agreement can be found with the experimental results in Figure 5a,b.

We then develop a real-time pulse detector for underwater healthcare management (Figure 5e), which successfully acquire a pulse frequency of 77 beats min^{-1} with time intervals of ≈0.78 ± 0.05 s for a volunteer. The pulse detector is so sensitive that the captured information even contains three distinguishable peaks, corresponding to percussion wave (P1), tidal wave (P2) and diastolic wave (P3), which are the keys to diagnosis the arterial stiffness and vascular aging related healthcare issues (inset of Figure 5e).[43,44] A underwater handwriting recognition system (Figure 5f) is assembled by sandwiching a SGC layer between two polyethylene terephthalate (PET) films, to explore the waterproof anti-counterfeiting applications. In Figure 5g, the SGC based underwater handwriting system can generate dedicated $\Delta R/R_0$ signals in response to different letter. Moreover, the system can produce unique $\Delta R/R_0$waveforms for the same letter written by different individuals (Figure S31, Supporting Information), indicating a remarkable promise in machine learning and artificial intelligence.

A tactical trajectory tracking board is developed to trace the dynamic pressure distribution in real time at underwater environment. A sensing matrix consisting of a 16 pixels array (4 × 4 SGC sensing units), was designed and assembled with a VHB tape substrate, conductive silver wires and a PET film cover layer (**Figure 6**a). When the finger touches the sensing

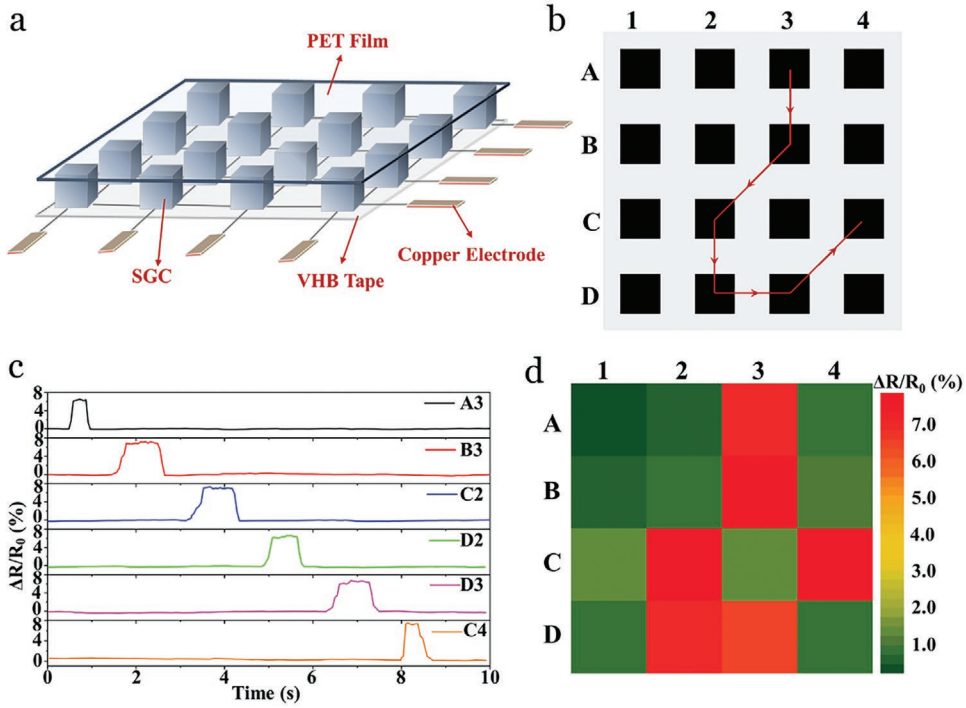

Figure 6. The underwater tactile trajectory tracking board. a) Schematic illustration of 4 × 4 SGC unit array. b) Diagram of the trajectory of finger movement. c) The output corresponding $\Delta R/R_0$ signals in sequence. d) The corresponding mapping of the magnitudes of output $\Delta R/R_0$.

matrix in the order as shown in Figure 6b, each sensor unit will produce corresponding $\Delta R/R_0$ signals in sequence. Figure 6c depicts that the sensing units exhibit various starting response time, time intervals between two sensing units and duration of outputted signals. Accompanying with the magnitudes of stress reflected by distinct colors in the real-time mapping (Figure 6d), the sensing matrix can intuitively realize spatially resolved tactile trajectory, by identifying the dynamic tactile trajectory. The trajectory tracking system remains fully functional even after being immersed in water for 3 months (Figure S32, Supporting Information).

3. Conclusion

In this work, we describe a structural gel composite approach by creating a hydrophobic Lipogel thin layer on the surface of conductive hydrogel/Mxene, then develop a robust sensing strategy with unique water proof feature to be used at underwater environment. Benefiting from the water isolation function fulfilled by the hydrophobic Lipogel layer and the strong covalent bond on the Lipogel/hydrogel interface, the SGC can be empowered with ultra-stability for mechanical and electrical properties both in the open air and aquatic environment. High sensitivity (GF of 14.5) has been facilitated for SGC based sensors through the construction of electronic transmission pathways in hydrogel/MXene core and preservation of conductive core from the Lipogel layer. Moreover, the SGC-based sensor shows tremendous potentials in real-time underwater sensing applications, such as human motion detection for healthcare management, smart writing system with waterproof anti-counterfeiting feature and tactile trajectory tracking. We expect this work to shed extra light on designing and developing future hydrogel-based smart microelectronic system for underwater or aquatic environment.

4. Experimental Section

Fabrication of MXene ($Ti_3C_2T_x$) Nanosheets: The delaminated MXene was prepared via the reported method.[45] As shown in Figure S2a (Supporting Information), Ti_3AlC_2 (1 gram) was slowly added into the etching solution consisting of 1.6 g LiF and 20 mL 9M HCl, and stirred for 24 h at 40 °C. The suspension was subsequently rinsed with DI water to obtain the multilayered $Ti_3C_2T_x$. Then, the $Ti_3C_2T_x$ was dispersed into water and sonicated for 1 h at the ice bath under N_2 protection. The supernatant was collected by centrifuging the mixed solution at 3500 rpm for 1 h. The obtained supernatant was the delaminated MXene dispersion with 4.8 wt‰, to be used in the subsequent experiments.

Preparation of Pristine Conductive Hydrogel: AA (6 mL) and HEA (2 mL) were added into DI water (20 mL), and sonicated for 5 min. Then, 30 mg APS was dissolved into the above solution and stirring for 20 min. Finally, the fabricated MXene aqueous solution (2.5 mL) was added to the mixed solution under stirring (Table S3, Supporting Information). The hydrogel was obtained after transferring into a rectangular glass mold (40 × 20 × 10 mm) and waiting for 20 min. The prepared conductive hydrogel was defined as PAHM-*x*%, where *x*% is the weight ratio of MXene solution to the hydrogel. If not specified, the conductive hydrogel/MXene refers to the PAHM-8%.

Surface Modification of Conductive Hydrogel: The modification process was to introduce double bonds on hydrogel/MXene surface based on the reaction between acryloyl chloride and hydroxyl groups.[35] First, the conductive hydrogel/MXene was immersed in acetone for 5–10 s to remove surface moisture and avoid the reaction between acryl chloride and water. Subsequently, the conductive hydrogel/MXene was immediately put into 20 mL ethyl acetate solvent with 6 mL triethylamine acid acceptor, and 5 mL acryloyl chloride was dripped slowly and reacted for 1 h in N_2 environment. When the reaction completed, the conductive hydrogel/MXene was obtained by rinsing with water and drying with N_2.

Preparation of Structural Gel Composite: The SGC was synthesized by in situ polymerization on the conductive hydrogel grafted with double bonds. 2.8 mL of B and 2.5 mL of L were added to 2.4 mL paraffin oil and mixed evenly. Then, crosslinking agent (14 µL of EGDMA) and photoinitiator (20 µL of DEAP) were added to above mixture, and stirred for 10 min to form the Lipogel precursor solution (Table S4, Supporting Information). After that, as shown in Figure S33 (Supporting Information), the conductive hydrogel/MXene modified with acryl chloride was placed on a transparent quartz glass, and fixed with rubber mold. The height of rubber mold was higher than that of hydrogel to facilitate the subsequent introduction of the Lipogel coating. Then the precursor of Lipogel (L/B-90%) was added to the hydrogel/MXene surface and covered with quartz glass. Next, UV irradiation was performed for 30 min to construct the Lipogel coating with the thickness of ≈100 µm on the surface of conductive hydrogel/MXene. The same operation was applied to the other 5 surfaces of the conductive hydrogel to form the complete coating. The thickness of Lipogel coating was controlled by adjusting the height of rubber mold. The dimension of SGC sample was 40 × 20 × 3 mm. If not specified, the SGC refers to the hydrogel of PAHM-8% and the Lipogel with L/B-90%. All human sensing demonstrations were performed in Xi'an Jiaotong University (China), where the project was fully assessed and approved by the university ethic committee with the consent issued from the participant.

Supporting Information

Supporting Information is available from the Wiley Online Library or from the author.

Acknowledgements

This work was supported partially by the China Postdoctoral Science Foundation (2020M683469), the National Natural Science Foundation of China (No. 22178278), Young Talent Support Plan of Xi'an Jiaotong University (China), and the Engineering and Physical Sciences Research Council (EPSRC, UK) grant EP/N007921. The authors also want to thank the Instrument Analysis Center of Xi'an Jiaotong University for their experimental support.

Conflict of Interest

The authors declare no conflict of interest.

Data Availability Statement

The data that support the findings of this study are available in the supplementary material of this article.

Keywords

gel composite, interface engineering, mechanosensing, tactical sensing, wearable electronics

Received: February 3, 2022
Revised: February 27, 2022
Published online:

[1] Y. S. Zhang, A. Khademhosseini, *Science* **2017**, *356*, 6337.
[2] Z. Lei, P. Wu, *Nat. Commun.* **2018**, *9*, 1134.
[3] X. Liu, J. Liu, S. Lin, X. Zhao, *Mater. Today* **2020**, *36*, 102.
[4] T. J. Wallin, J. Pikul, R. F. Shepherd, *Nat. Rev. Mater.* **2018**, *3*, 84.
[5] Z. Sun, Y. Yamauchi, F. Araoka, Y. S. Kim, J. Bergueiro, Y. Ishida, Y. Ebina, T. Sasaki, T. Hikima, T. Aida, *Angew. Chem., Int. Ed.* **2018**, *57*, 15772.
[6] B. B. Xu, Q. Liu, Z. Suo, R. C. Hayward, *Adv. Funct. Mater.* **2016**, *26*, 3218.
[7] Y. Liu, A. Sun, S. Sridhar, Z. Li, Z. Qin, J. Liu, X. Chen, H. Lu, B. Z. Tang, B. B. Xu, *ACS Appl. Mater. Interfaces* **2021**, *13*, 36361.
[8] L. Pan, G. Yu, D. Zhai, H. R. Lee, W. Zhao, N. Liu, H. Wang, B. C. Tee, Y. Shi, Y. Cui, Z. Bao, *Proc. Natl. Acad. Sci. USA* **2012**, *109*, 9287.
[9] W. Zhang, P. Feng, J. Chen, Z. Sun, B. Zhao, *Prog. Polym. Sci.* **2019**, *88*, 220.
[10] Y. Guo, J. Bae, Z. Fang, P. Li, F. Zhao, G. Yu, *Chem. Rev.* **2020**, *120*, 7642.
[11] C. Yang, Z. Suo, *Nat. Rev. Mater.* **2018**, *3*, 125.
[12] W. Zhang, B. Wu, S. Sun, P. Wu, *Nat. Commun.* **2021**, *12*, 4082.
[13] Y.-Z. Zhang, H. Lee Kang, H. Anjum Dalaver, R. Sougrat, Q. Jiang, H. Kim, N. Alshareef Husam, *Sci. Adv.* **2018**, *4*, eaat0098.
[14] S. Ji, C. Wan, T. Wang, Q. Li, G. Chen, J. Wang, Z. Liu, H. Yang, X. Liu, X. Chen, *Adv. Mater.* **2020**, *32*, 2001496.
[15] Y. Niu, H. Liu, R. He, Z. Li, H. Ren, B. Gao, H. Guo, G. M. Genin, F. Xu, *Mater. Today* **2020**, *41*, 219.
[16] F. Wu, Y. Pang, J. Liu, *Nat. Commun.* **2020**, *11*, 4502.
[17] H. Kamata, Y. Akagi, Y. Kayasuga-Kariya, U.-i. Chung, T. Sakai, *Science* **2014**, *343*, 873.
[18] J. Liu, Z. Chen, Y. Chen, H. U. Rehman, Y. Guo, H. Li, H. Liu, *Adv. Funct. Mater.* **2021**, *31*, 2101464.
[19] M. T. I. Mredha, S. K. Pathak, V. T. Tran, J. Cui, I. Jeon, *Chem. Eng. J.* **2019**, *362*, 325.
[20] X. Liu, Q. Zhang, G. Gao, *ACS Nano* **2020**, *14*, 13709.
[21] H. Fan, J. Wang, Z. Jin, *Macromolecules* **2018**, *51*, 1696.
[22] L. Xu, S. Gao, Q. Guo, C. Wang, Y. Qiao, D. Qiu, *Adv. Mater.* **2020**, *32*, 2004579.
[23] J. Wei, Y. Zheng, T. Chen, *Mater. Horiz.* **2021**, *8*, 2761.
[24] B. Yiming, X. Guo, N. Ali, N. Zhang, X. Zhang, Z. Han, Y. Lu, Z. Wu, X. Fan, Z. Jia, S. Qu, *Adv. Funct. Mater.* **2021**, *31*, 2102773.
[25] Z. Yu, P. Wu, *Adv. Mater.* **2021**, *33*, 2008479.
[26] K. Kikuchi, S. Shigeta, K. Numayama-Tsuruta, T. Ishikawa, *Int. J. Pharm.* **2020**, *587*, 119708.
[27] K. S. Wu, M. M. Stefik, K. P. Ananthapadmanabhan, R. H. Dauskardt, *Biomaterials* **2006**, *27*, 5861.
[28] H. Yuk, T. Zhang, G. A. Parada, X. Liu, X. Zhao, *Nat. Commun.* **2016**, *7*, 12028.
[29] T. Zhu, C. Jiang, M. Wang, C. Zhu, N. Zhao, J. Xu, *Adv. Funct. Mater.* **2021**, *31*, 2102433.
[30] M. T. I. Mredha, H. H. Le, J. Cui, I. Jeon, *Adv. Sci.* **2020**, *7*, 1903145.
[31] X. Yao, L. Chen, J. Ju, C. Li, Y. Tian, L. Jiang, M. Liu, *Adv. Mater.* **2016**, *28*, 7383.
[32] P. Maier Greg, V. Rapp Michael, J. H. Waite, N. Israelachvili Jacob, A. Butler, *Science* **2015**, *349*, 628.
[33] H. Yuk, C. E. Varela, C. S. Nabzdyk, X. Mao, R. F. Padera, E. T. Roche, X. Zhao, *Nature* **2019**, *575*, 169.
[34] G. Ge, Y. Z. Zhang, W. Zhang, W. Yuan, J. K. El-Demellawi, P. Zhang, E. Di Fabrizio, X. Dong, H. N. Alshareef, *ACS Nano* **2021**, *15*, 2698.
[35] T. Zhao, G. Wang, D. Hao, L. Chen, K. Liu, M. Liu, *Adv. Funct. Mater.* **2018**, *28*, 1800793.
[36] H. Gao, Z. Zhao, Y. Cai, J. Zhou, W. Hua, L. Chen, L. Wang, J. Zhang, D. Han, M. Liu, L. Jiang, *Nat. Commun.* **2017**, *8*, 15911.
[37] S. Wang, S. Vajjala Kesava, E. D. Gomez, M. L. Robertson, *Macromolecules* **2013**, *46*, 7202.
[38] V. Tirtaatmadja, K. C. Tam, R. D. Jenkins, *Macromolecules* **1997**, *30*, 3271.
[39] S. Das, P. Martin, G. Vasilyev, R. Nandi, N. Amdursky, E. Zussman, *Macromolecules* **2020**, *53*, 11130.

[40] Z. Zhang, L. Wang, H. Yu, F. Zhang, L. Tang, Y. Feng, W. Feng, *ACS Appl. Mater. Interfaces* **2020**, *12*, 15657.
[41] H. Wei, Z. Wang, H. Zhang, Y. Huang, Z. Wang, Y. Zhou, B. B. Xu, *Chem. Mater.* **2021**, *33*, 6731.
[42] Y. Ma, Y. Gao, L. Liu, X. Ren, G. Gao, *Chem. Mater.* **2020**, *32*, 8938.
[43] W. W. Nichols, *Am. J. Hypertens.* **2005**, *18*, 3S.
[44] Y. Yao, L. Hao, L. Xu, Y. Zhang, L. Qi, Y. Sun, B. Yang, F. N. van de Vosse, Y. Yao, *Sci. Rep.* **2017**, *7*, 5864.
[45] M. Ghidiu, M. R. Lukatskaya, M. Q. Zhao, Y. Gogotsi, M. W. Barsoum, *Nature* **2014**, *516*, 78.